Emerging Microbes & Infections
2021, VOL. 10
https://doi.org/10.1080/22221751.2021.1899770

OPEN ACCESS Check for updates

The preclinical inhibitor GS441524 in combination with GC376 efficaciously inhibited the proliferation of SARS-CoV-2 in the mouse respiratory tract

Yuejun Shi [a,c]*, Lei Shuai [b]*, Zhiyuan Wen [b], Chong Wang [b], Yuanyuan Yan [a,c], Zhe Jiao [a,c], Fenglin Guo [a,c], Zhen F. Fu [a,c], Huanchun Chen [a,c], Zhigao Bu [b,d] and Guiqing Peng [a,c]

[a]State Key Laboratory of Agricultural Microbiology, College of Veterinary Medicine, Huazhong Agricultural University, Wuhan, People's Republic of China; [b]State Key Laboratory of Veterinary Biotechnology, Harbin Veterinary Research Institute, Chinese Academy of Agricultural Sciences, Harbin, People's Republic of China; [c]Key Laboratory of Preventive Veterinary Medicine in Hubei Province, The Cooperative Innovation Center for Sustainable Pig Production, Huazhong Agricultural University, Wuhan, People's Republic of China; [d]National High Containment Laboratory for Animal Diseases Control and Prevention, Harbin, People's Republic of China

ABSTRACT

The unprecedented coronavirus disease 2019 (COVID-19) pandemic, caused by severe acute respiratory syndrome coronavirus 2 (SARS-CoV-2), is a serious threat to global public health. Development of effective therapies against SARS-CoV-2 is urgently needed. Here, we evaluated the antiviral activity of a remdesivir parent nucleotide analog, GS441524, which targets the coronavirus RNA-dependent RNA polymerase enzyme, and a feline coronavirus prodrug, GC376, which targets its main protease, using a mouse-adapted SARS-CoV-2 infected mouse model. Our results showed that GS441524 effectively blocked the proliferation of SARS-CoV-2 in the mouse upper and lower respiratory tracts via combined intranasal (i.n.) and intramuscular (i.m.) treatment. However, the ability of high-dose GC376 (i.m. or i.n. and i.m.) was weaker than GS441524. Notably, low-dose combined application of GS441524 with GC376 could effectively protect mice against SARS-CoV-2 infection via i.n. or i.n. and i.m. treatment. Moreover, we found that the pharmacokinetic properties of GS441524 is better than GC376, and combined application of GC376 and GS441524 had a synergistic effect. Our findings support the further evaluation of the combined application of GC376 and GS441524 in future clinical studies.

ARTICLE HISTORY Received 16 November 2020; Revised 17 February 2021; Accepted 19 February 2021

KEYWORDS SARS-CoV-2; mouse model; preclinical inhibitor; combined application; antiviral efficacy

Introduction

Severe acute respiratory syndrome coronavirus 2 (SARS-CoV-2) causes coronavirus disease 2019 (COVID-19), which spread rapidly to more than 235 countries. The number of infections has exceeded 100 million, and more than 2 million deaths were reported (https://www.who.int/emergencies/diseases/novel-coronavirus-2019). The World Health Organization (WHO) declared COVID-19 a global health emergency. Multiple vaccine candidates and therapeutics are in clinical trials [1–6], and effective treatments or cures for COVID-19 are still urgently needed.

Coronaviruses are enveloped, positive-sense, single-stranded RNA viruses, and their genomic RNA is approximately 30 kb and contains at least 6 open reading frames (ORFs) [7]. The first ORF (ORF 1a/b) encodes two polyproteins, pp1a and pp1ab, and these polyproteins are processed via a main protease (M^{pro}, also known as the 3C-like protease) and one or two papain-like proteases (PLPs) into 16 nonstructural proteins (nsps) [8,9]. These nsps engage in the production of subgenomic RNAs that encode four main structural proteins [envelope (E), membrane (M), spike (S), and nucleocapsid (N) proteins] and other accessory proteins [8,9]. Among these nsps, M^{pro} and nsp12 (RdRp) of SARS-CoV-2 are functionally and structurally conserved among these viruses and essential for viral replication; they are considered a potential target for the design of antiviral drugs [10–17].

GC376, a dipeptidyl bisulfite adduct salt, exerts strong inhibitory effects on picornaviruses and coronaviruses [11–19]. The latest research has shown that GC376 can also inhibit the replication of SARS-CoV-2 in Vero E6 cells [12,13,16]. Moreover, antiviral treatment with GC376 led to a full recovery in laboratory cats with feline infectious peritonitis (FIP) caused by feline coronavirus (FIPV) [19]. Currently, no studies have evaluated the ability of GC376 to inhibit SARS-CoV-2 in animals. In addition, remdesivir

CONTACT Zhigao Bu buzhigao@caas.cn; Guiqing Peng penggq@mail.hzau.edu.cn
*These authors contributed equally to this work.
Supplemental data for this article can be accessed https://doi.org/10.1080/22221751.2021.1899770

© 2021 The Author(s). Published by Informa UK Limited, trading as Taylor & Francis Group.
This is an Open Access article distributed under the terms of the Creative Commons Attribution License (http://creativecommons.org/licenses/by/4.0/), which permits unrestricted use, distribution, and reproduction in any medium, provided the original work is properly cited.

(RDV) and its parent nucleoside analog GS-441524 inhibit CoVs (including SARS-CoV-2) and other viruses [20–31]. However, latest research showed that RDV was not intended for lung-specific delivery, and GS-441524 is the predominant metabolite that reaches the lungs, which suggests that GS-441524 is superior to RDV for COVID-19 treatment [24,27].

Because GC376 and GS441524 target the key proteases M^{pro} and RdRp of SARS-CoV-2 replication [10,12,13,16], respectively, their combined application may be more effective in the treatment of COVID-19. The combined application of GC376 with RDV produced additive sterilizing additive effects against SARS-CoV-2 in Vero E6 cells [13]. However, the efficacy of the combined application of GC376 and GS441524 in the inhibition of SARS-CoV-2 replication was not investigated *in vivo* and *in vitro*. Our team generated a mouse-adapted SARS-CoV-2 (HRB26M) that efficiently replicates in the upper and lower respiratory tract in BALB/c mice [4,26]. Hence, we assessed the antiviral efficacy of GC376 and GS441524 in an HRB26M-infected BALB/c mouse model. Our results showed that GC376, which effectively inhibited the virus at the cellular level, was less effective *in vivo*. The ability of GS441524 to block the proliferation of SARS-CoV-2 was significantly higher than GC376 in mice. Notably, the low-dose combined application of GC376 and GS441524 could effectively block SARS-CoV-2 infection in the mouse upper and lower respiratory tract.

Materials and methods

Compounds, cells, viruses and animal experiments

The compounds GC376 (molecular weight: 507.53 g/M) and GS441524 (molecular weight: 291.26 g/M) were synthesized at WuXi AppTec with purities higher than 95%. They were dissolved in 5% ethanol, 30% propylene glycol, 45% PEG 400, and 20% water with a concentration of 40 mM/l according to a previously described study [31].

Vero E6 cells (African green monkey kidney, ATCC) were maintained in Dulbecco's modified Eagle's medium (DMEM, Thermo Scientific, USA) containing 10% fetal bovine serum (Thermo Scientific, USA) and antibiotics, and incubated at 37°C with 5% CO_2 [4]. In addition, SARS-CoV-2/HRB26/human/2020/CHN (HRB26, GISAID access no. EPI_ISL_459909) and Mouse-adapted SARS-CoV-2/HRB26/human/2020/CHN (HRB26M, GISAID access no. EPI_ISL_459910) were obtained following the previous method [26]. Infectious virus titres were determined using a plaque forming unit (PFU) assay in Vero E6 cells, and virus stocks were stored in aliquots at −80 °C until use.

Specific pathogen-free female BALB/c mice, aged 4–6 weeks were obtained from Beijing Vital River Laboratory Animal Technologies Co., Ltd (Beijing, China) and were housed and bred in the temperature-, humidity- and light cycle-controlled animal facility (20 ± 2°C; 50 ± 10%; light, 7:00–19:00; dark, 19:00-7:00, respectively) of the Animal Center, Academy of Military Medical Sciences, Beijing.

Protein expression and purification

SARS-CoV-2 M^{pro} flanked by an N-terminal His6 tag was cloned into pET-32a (+). For expression of SARS-CoV-2 M^{pro}, the preserved *Escherichia coli (E. coli)* strain BL21 (DE3, including M^{pro} plasmids) (from Sheng-ce Tao lab) were cultured at 37°C in LB medium containing 50 μg/ml ampicillin. Protein expression was induced with 0.8 mM isopropyl β-D-1-thiogalactopyranoside (IPTG) when the culture density reached an OD_{600} of 0.8, and cell growth continued for an additional 16 h at 18°C. Protein purification was performed as described previously [32,33]. Briefly, the cell supernatant was filtered with a 0.45-μm filter and loaded onto a nickel-charged HisTrap HP column (GE Healthcare). Proteins were eluted with elution buffer (20 mM Tris-HCl, 500 mM NaCl and 500 mM imidazole, pH 7.4). Then, the harvested protein was concentrated to approximately 2.0 ml and filtered using a Superdex 200 gel filtration column (GE Healthcare) equilibrated with buffer (20 mM Tris-HCl and 200 mM NaCl, pH 7.4). For crystallization, the purified protein was concentrated to approximately 8 mg/ml, flash frozen with liquid nitrogen, and stored at −80°C. The concentration of purified SARS-CoV-2 M^{pro} was determined by the absorbance at 280 nm (A_{280}) using a NanoDrop 2000c UV-Vis spectrophotometer (Thermo Fisher Scientific).

Crystallization, data collection and structure determination

GC376 and M^{pro} (8 mg/ml) were incubated at room temperature for 1 h (molar ratio: 2:1), and the complex was crystallized by the hanging drop vapour diffusion method at 20°C. The best crystallization conditions for the complex were in hanging drops consisting of 2 μl of reservoir solution (0.1 M sodium malonate pH 6.0, 12% w/v polyethylene glycol 3,350) and 2 μl of the complex in 20 mM Tris-HCl and 200 mM NaCl, pH 7.4, followed by incubation at 20°C for 3 days. Then, the crystals were flash-cooled in liquid nitrogen in a cryoprotectant solution containing 30% ethylene glycol and 70% reservoir solution (0.1 M sodium malonate pH 6.0, 14% w/v polyethylene glycol 3,350). Data collection was performed at the research associates at Center for Protein

Research (CPR), Huazhong Agricultural University (wavelength = 1.5418 Å, temperature = 100 K). Reflections were integrated, merged, and scaled using HKL-3000 [34], and the resulting statistics are listed in Supplemental Table 1. The structure was solved by molecular replacement with PHASER (Phenix, Berkeley, CA, USA) [35] using the structure of the SARS-CoV-2 M^{pro} (PDB identifier 7BQY) as a starting model. Manual model rebuilding and refinement were performed using COOT [36] and the PHENIX software suite. Structural figures were generated using PyMOL (Schrödinger). Detailed molecular interactions were determined using LIGPLOT [37].

Evaluation of antiviral activity in Vero e6 cells

Cell viability was determined using the Cell Titer-Glo kit (Promega, Madison, WI, USA) following the manufacturer's instructions. Briefly, Vero E6 cells were seeded in 96-well plates with opaque walls. After 12–16 h, the indicated concentrations of GC376 (0, 1, 5, 10, 50, 100, 500 μM), GS441524 (0, 1, 5, 10, 50, 100, 500 μM) and GC376 + GS441524 (0, 0.5, 2.5, 5, 25, 50, 250 μM) were added for 24 h. Cell Titer-Glo reagent was added to each well, and luminescence was measured using a GloMax 96 Microplate Luminometer (Promega, Madison, WI, USA).

Antiviral activity experiment was determined following a previous method [26]. Briefly, Vero E6 cells were pretreated with the indicated concentrations of GC376 (0, 0.5, 1, 2, 4, 6, 8, 10 μM), GS441524 (0, 0.5, 1, 2, 4, 6, 8, 10 μM) and GC376 + GS441524 (0, 0.25, 0.5, 1, 2, 3, 4, 5 μM) or with vehicle solution (12% sulfobutylether-β-cyclodextrin, pH 3.5) alone for 1 h. The cells were then infected with HRB26 or HRB26M at an MOI of 0.005 and incubated for 1 h at 37°C. The cells were washed with PBS, and virus growth medium containing the indicated amounts of GC376, GS441524 and GC376 + GS441524 or vehicle solution alone was added. The supernatants were collected at 24 h p.i. for viral titration by a PFU assay in Vero E6 cells. Relative viral titres were calculated on the basis of the ratios to the viral titres in the mock-treated counterparts. The data were analyzed using GraphPad Prism 7.0. The results are shown as the mean values with standard deviations of three independent experiments.

In vivo *toxicity study of GC376 and GS441524*

The toxicity studies were performed in 4- to 6-week-old female BALB/c mice. BALB/c mice were assigned to four groups (five mice per group), one mock group (i.m. administration of solvent) and three i.m. administered groups: GC376 (40 mM/l, 100 μl), GS441524 (40 mM/l, 100 μl) and GC376 + GS441524 (20 mM/l, 100 μl), respectively. Mice in the mock and experimental groups were weighed daily for 15 days. In addition, blood samples were collected at 0, 5, 10 and 15 days after administration. Various blood chemistry values or blood cell counts were performed at Wuhan Servicebio Biological Technology Co., Ltd. The data were analyzed using GraphPad Prism 7.0.

In vivo *antiviral study of GC376 and GS441524*

Firstly, groups of six 4- to 6-week-old female BALB/c mice were treated i.m. with a loading dose of GC376 (40 or 8 mM/l, 100 μl), GS441524 (40 or 8 mM/l, 100 μl) and GC376 + GS441524 (20 or 4 mM/l, 100 μl), followed by a daily maintenance dose. Alternatively, mice were treated intranasally with a single treatment (GC376, 20 mM/l, 50 μl; GS441524, 20 mM/l, 50 μl; GC376 + GS441524, 10 mM/l, 50 μl) or a combination of GC376 (20 mM/l, 50 μl, i.n. and 40 mM/l, 100 μl, i.m.), GS441524 (20 mM/l, 50 μl, i.n. and 40 mM/l, 100 μl, i.m.) and GC376 + GS441524 (10 mM/l, 50 μl, i.n. and 20 mM/l, 100 μl, i.m.), followed by a daily maintenance dose. As a control, mice were administered vehicle solution (12% sulfobutylether-β-cyclodextrin, pH 3.5) daily. One hour after administration of the loading dose of GC376, GS441524 and GC376 + GS441524 or vehicle solution, each mouse was inoculated intranasally with$10^{3.6}$ PFU of HRB26M in 50 μl. Three mice from each group were euthanized on days 3 and 5 p.i. The nasal turbinates and lungs were collected for viral detection by qPCR and PFU assay according to previously described methods [4,26]. The amount of vRNA for the target SARS-CoV-2 N gene was normalized to the standard curve from a plasmid (pBluescript II SK-N, 4,221 bp) containing the full-length cDNA of the SARS-CoV-2 N gene. The assay sensitivity was 1000 copies/ml. The data were analyzed using Microsoft Excel 2016 and GraphPad Prism 7.0.

Pharmacokinetics study of GC376 and GS441524 in BALB/c mice and SD rats

Healthy SPF BALB/c mice (7-8 weeks) and SD rats (4-6 weeks) were used in a single-dose PK study. At time point zero, the BALB/c mice and SD rats of groups A, B and C (each group including twenty BABL/c mice or five SD rats) received i.m. injections of GC376 (111 mg/kg), GS441524 (67 mg/kg) and GC376 + GS441524 (55.5 + 33.5 mg/kg), which are the same doses according to *in vivo* antiviral study. The blood was collected at 0, 0.083, 0.25, 0.5, 1, 2, 4, 8, 12 and 24 h and placed in a precooled polypropylene centrifuge tube containing 3.0 μl of 40% EDTAK2. Then, the whole blood was centrifuged at 7800 g/min for 10 min at 4°C. Plasma was collected and stored in a freezer at −80°C. Plasma drug concentration was analyzed using LC-MS/MS. Pharmacokinetic parameters

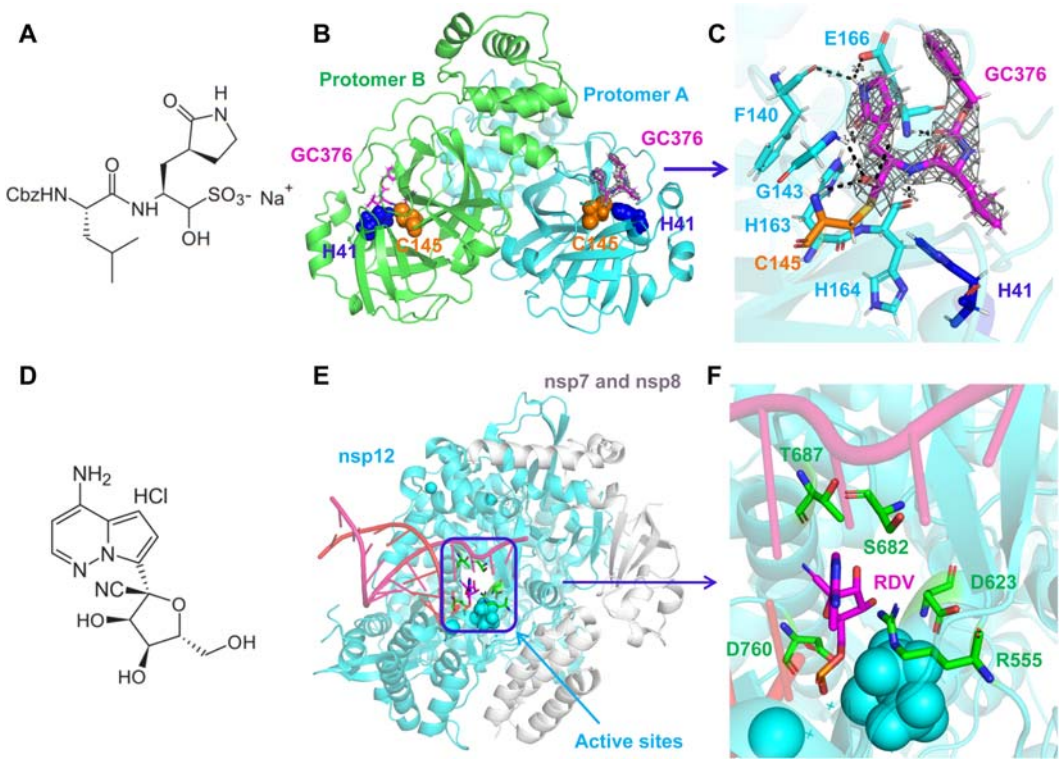

Figure 1. Structural analysis of GC-376 and GS441524 targeting SARS-CoV-2 M^{pro} and RdRp. (A) The dipeptidyl protease inhibitor, GC376. (B) Crystal structure of SARS-CoV-2 M^{pro} in complex with GC376. (C) GC376 interacts covalently with the active cysteine site of SARS-CoV-2 M^{pro}. Electron density at 1.5 σ is shown in grey mesh. Hydrogen bonds are shown as black dashed lines. (D) The chemical structure of GS-441524. (E) Cryo-EM structure of the apo nsp12-nsp-7-nsp8 RdRp complex (PDB ID: 7BV2). (F) Enlarged view of the active sites, depicting the interaction between RDV and surrounding amino acids.

were calculated using WinNonlin software (version 6.4), and a non-atrioventricular model was used for data fitting. The data were analyzed using Microsoft Excel 2016 and GraphPad Prism 7.0.

Ethics statement, biosafety and facility

All of the mice used in this study were maintained in compliance with the recommendations in the Regulations for the Administration of Affairs Concerning Experimental Animals made by the Ministry of Science and Technology of China. The toxicity study and single-dose PK study were performed using protocols that were approved by the Scientific Ethics Committee of Huazhong Agricultural University (permit number: HZAURA-2020-0007 and HZAUMO-2020-0008). All experiments with infectious SARS-CoV-2 were performed in the biosafety level 4 and animal biosafety level 4 facilities in the Harbin Veterinary Research Institute (HVRI) of the Chinese Academy of Agricultural Sciences (CAAS), which are approved for this use by the Ministry of Agriculture and Rural Affairs of China.

Statistical analysis

Statistical analysis was carried out using GraphPad Prism 7.0. Statistical significance was determined using an unpaired two-tailed Student's t test. Data are presented as mean values ±SD (95% confidence interval). *, $P < 0.05$ was considered statistically significant; **, $P < 0.01$ was considered highly significant; ***, $P < 0.001$ and ****, $P < 0.0001$ were considered extremely significant. All experiments were further confirmed using biological repeats.

Data availability

Coordinates and structural factors for SARS-CoV-2 M^{pro} in complex with GC376 were deposited in the Protein Data Bank with accession number 7CBT. Other data supporting the findings of this study are available within the paper and its Supplementary Information files, or upon reasonable request from the corresponding author.

Results and discussion

Structural analysis of GC376 and GS441524 targeting SARS-CoV-2 M^{pro} and nsp12 (RdRp)

In this study, we first analyzed the mechanism by which GC376 and GS441524 inhibit SARS-CoV-2 replication through structural biology methods. GC376 (Figure 1A) is a preclinical inhibitor against feline infectious peritonitis virus (FIPV) [17,19,38] that has become a broad-spectrum prodrug targeting

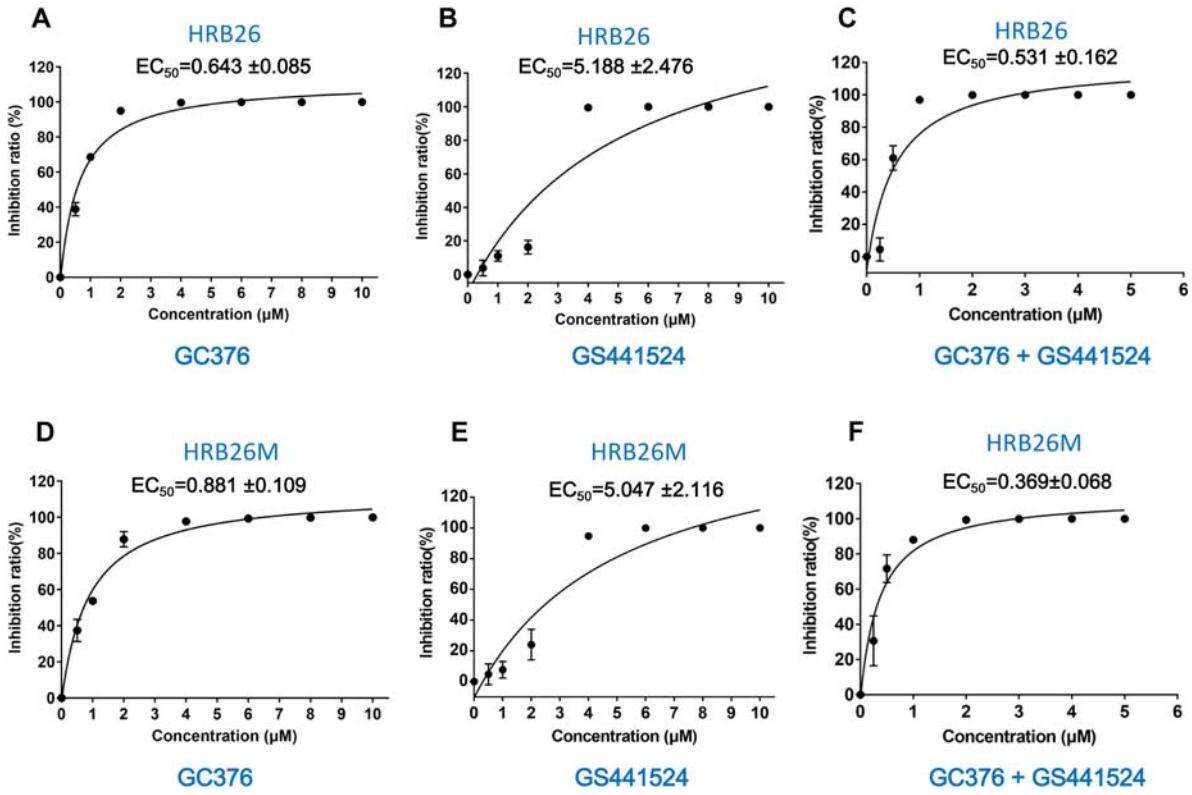

Figure 2. GC376 and GS441524 potently inhibit SARS-CoV-2 in Vero E6 cells. (A-C) Percent inhibition of SARS-CoV-2 (HRB26) by GC376, GS441524 and GC376 + GS441524 in Vero E6 cells. (D-F) Percent inhibition of SARS-CoV-2 (HRB26M) by GC376, GS441524 and GC376 + GS441524 in Vero E6 cells. The concentrations of GC376 and GS441524 ranged from 0 to 10 μM. The 50% inhibitory concentration (EC_{50}) was calculated using GraphPad Prism 7.0. The error bars show the S.D. of the results from three replicates.

coronavirus M^{pro} [14,39,40]. We determined the high-resolution crystal complex structure of M^{pro} with GC376 at a resolution of 2.35 Å (Supplemental Table 1). The crystal of M^{pro}-GC376 belongs to the space group P1211, and an asymmetric unit contains two molecules (designated protomer A and protomer B) (Figure 1B). The structure of each protomer contains three domains with the substrate-binding site comprised of a His41-Cys145 dyad located in the cleft between domain I and II (Supplementary Figure 1). The electron density map clearly showed compound GC376 in the substrate binding pocket of the SARS-CoV-2 M^{pro}, and details of the interaction are shown in Figure 1C and Supplementary Figure 1. GC376 interacts with His41, Phe140, Leu141, Asn142, Ser144, Cys145, His163, His164, Met165, Glu166, His172, Asp187, Arg188 and Gln189 via many hydrogen bonds and hydrophobic interactions, and binds stably in the groove formed by domain I and domain II. Moreover, we found that GC376 is covalently attached to Cys145 as a hemithioacetal (Figure 1C), which prevents the binding and processing of M^{pro} to the substrate [12,16,39]. Additionally, GS441524 is the parent nucleoside of RDV (Figure 1D and Supplementary Figure 2A), and has shown broad-spectrum inhibition of the replication of various coronaviruses, including SARS-CoV-2 [24,31,41]. Since the mechanism by which GS441524 inhibits SARS-CoV-2 replication is similar to that of RDV [24,41], we showed the cryo-electron microscopy (cryo-EM) ternary structure of the complex with RDV (PDB: 7BV2) [10]. Previous studies have shown that RDV, like many nucleotide analog prodrugs, inhibits viral RdRp activity via nonobligate RNA chain termination [10,42,43]. In the complex structures, RMP mimics adenosine monophosphate (AMP) and forms standard Watson–Crick base pairs with uridine monophosphate (UMP) in the RNA template strand [10,44,45]. Moreover, we observed that RDV stably bound nsp12 through hydrophobic interactions with Arg555, Asp623, Ser682, Thr687 and Asp760 (Figure 1E, F and Supplementary Figure 2B).

Combined application of GC376 and GS441524 has an enhanced ability to inhibit SARS-CoV-2 in Vero E6 cells

We evaluated the inhibitory efficacy of GC376, GS441524 and the combined application of GC376 and GS441524 (molar ratio: 1:1) (GC376 + GS441524) on the replication of live virus (SARS-CoV-2: HRB26 and HRB26M) in Vero E6 cells. We first tested the cellular cytotoxicity of these compounds *in vitro*. GC376 and GS441524 did not produce obvious cytotoxicity at concentrations up to 250 μM in Vero E6 cells (CC_{50} > 250 μM; Supplementary Figure 3). Our results

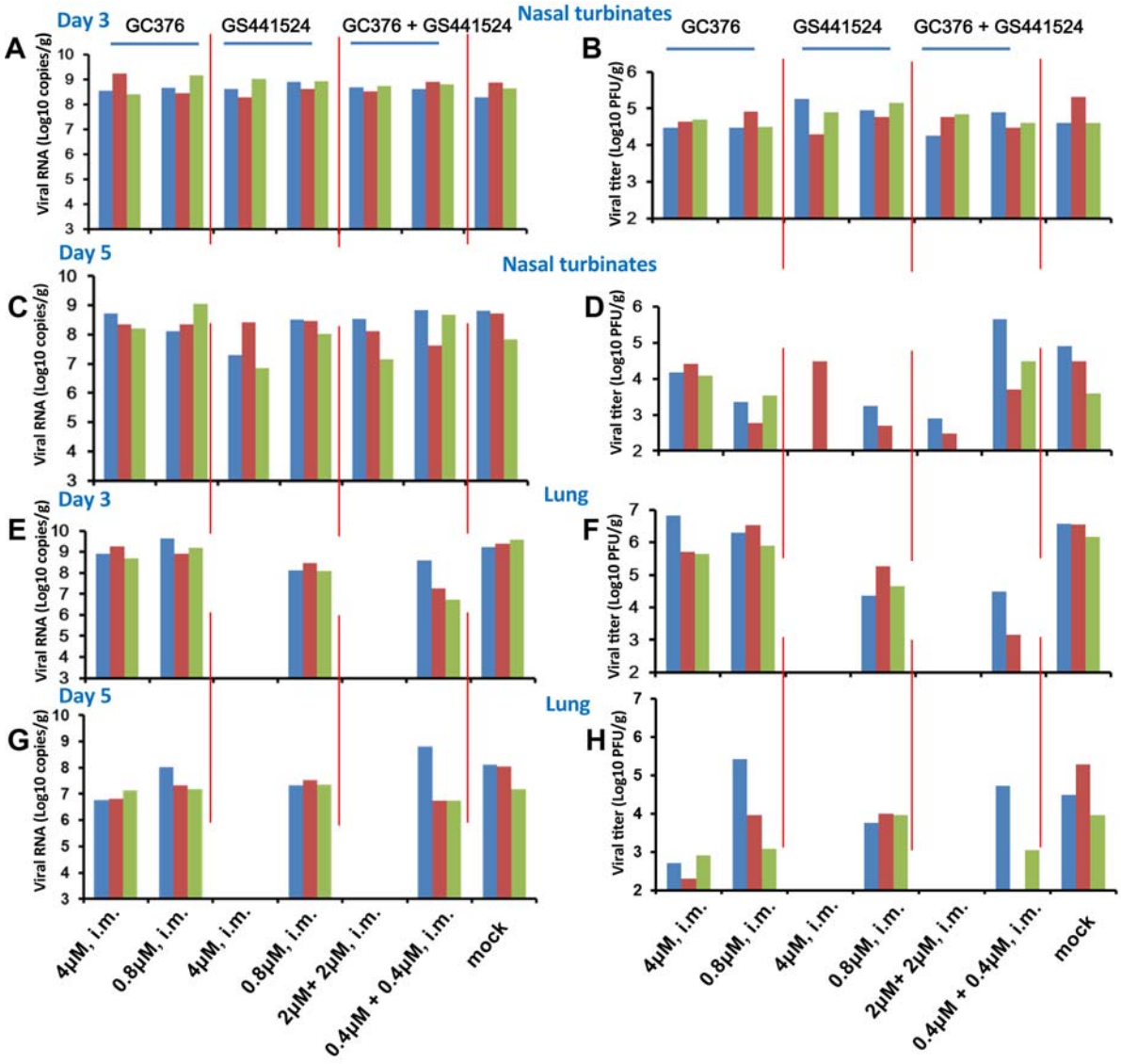

Figure 3. Evaluation of i.m. GC376, GS441524 and GC376 + GS441524 against SARS-CoV-2 infection in mice. Four- to six-week-old female BALB/c mice were intramuscularly administered a loading dose of GC376 (4 or 0.8 μM), GS441524 (4 or 0.8 μM), GC376 + GS441524 (2 μM + 2 μM or 0.4 μM + 0.4 μM), followed by a corresponding daily maintenance dose. Control mice were administered vehicle solution (12% sulfobutylether-β- cyclodextrin, pH 3.5) daily, in parallel (0 μM). One hour after administration of the loading dose of GC376, GS441524, GC376 + GS441524 or vehicle solution, the mice were inoculated intranasally with $10^{3.6}$ PFU of HRB26M in a volume of 50 μl. On days 3 and 5 p.i., three mice in each group were euthanized and their nasal turbinates and lungs were collected. The viral RNA copies and infectious titres in the nasal turbinates (A-D) and lungs (E-H) were detected by qPCR and viral titration. The concentrations of the daily maintenance doses are shown.

showed that GC376 and GS441524 were efficacious against HRB26, with 50% inhibitory concentration (EC_{50}) values of 0.643 ± 0.085 μM and 5.188 ± 2.476 μM, respectively (Figure 2A, B). GC376 and GS441524 were also efficacious against HRB26M, with EC_{50} values of 0.881 ± 0.109 μM and 5.047 ± 2.116 μM, respectively (Figure 2D, E). Our results showed that the ability of GC376 to inhibit viral (HRB26 and HRB26M) replication was better than GS441524 when the agents were applied alone. We observed that the GC376 + GS441524 more effectively inhibited HRB26 and HRB26M replication than single treatment, with EC_{50} values of 0.531 ± 0.162 μM and 0.369 ± 0.068 μM, respectively (Figure 2C, F). In the replication process of coronavirus, M^{pro} is one of the first nsps processed by the polyprotein, and other replication-related proteins, such as RdRp, can be produced with the participation of M^{pro} and PLP proteases [8,9]. This phenomenon may be the reason why GC376 is better than GS441524, and their combined application may result in a synergistic effect because these agents target different proteins involved in virus replication.

Low-dose GC376 + GS441524 could effectively protect mice from HRB26M infection in the upper and lower respiratory tracts

The potential toxicity of GC376, GS441524 and GC376 + GS441524 were evaluated in healthy specific pathogen-free (SPF) mice at 4–6 weeks. The mice were

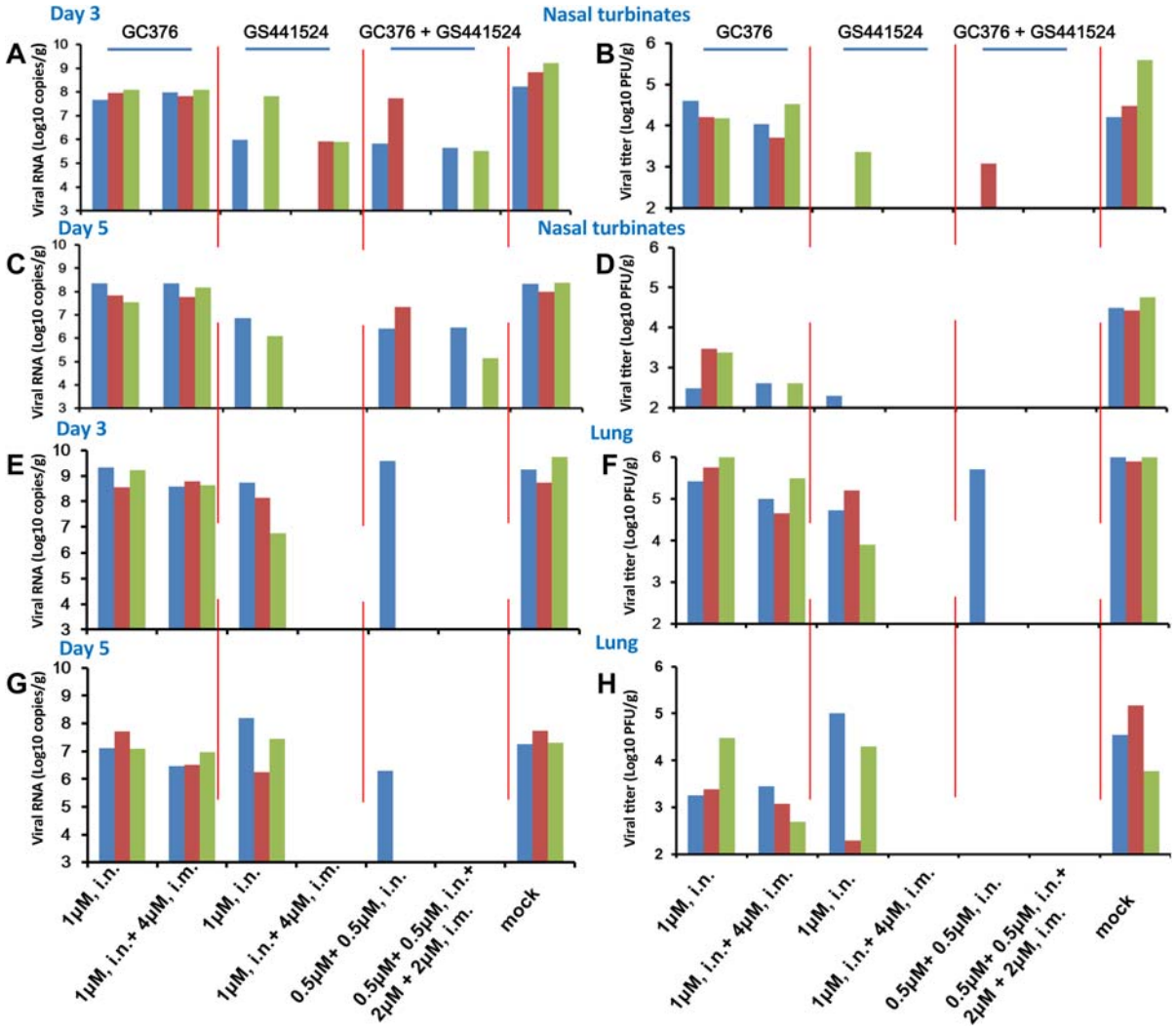

Figure 4. Evaluation of i.n. and i.m. GC376, GS441524 and GC376 + GS441524 against SARS-CoV-2 infection in mice. Four- to six-week-old female BALB/c mice were administered a loading dose of GC376 (1 μM, i.n. or 1 μM, i.n. + 4 μM, i.m.), GS441524 (1 μM, i.n. or 1 μM, i.n. + 4 μM, i.m.), GC376 + GS441524 (0.5 μM + 0.5 μM, i.n. or 0.5 μM + 0.5 μM, i.n. and 2 μM + 2 μM, i.m.), followed by a corresponding daily maintenance dose. Control mice were administered vehicle solution (12% sulfobutylether-β- cyclodextrin, pH 3.5) daily in parallel (0 μM). One hour after administration of the loading dose of GC376, GS441524, GC376 + GS441524 or vehicle solution, the mice were inoculated intranasally with $10^{3.6}$ PFU of HRB26M in a volume of 50 μl. On days 3 and 5 p.i., three mice in each group were euthanized and their nasal turbinates and lungs were collected. The viral RNA copies and infectious titres in the nasal turbinates (A-D) and lungs (E-H) were detected by qPCR and viral titration. The concentrations of the daily maintenance doses are shown.

intramuscularly (i.m.) administered GC376 (40 mM/l, 100 μl), GS441524 (40 mM/l, 100 μl) and GC376 + GS441524 (20 mM/l, 100 μl) for 15 days, and they were observed daily for adverse effects. During the study period, there were no clinically significant changes in vital signs (Supplementary Figure 4), indicating that the dose and administration route of GC376, GS441524 and GC376 + GS441524 were suitable for the *in vivo* efficacy study.

We assessed the antiviral efficacy of i.m. administered GC376 (40 or 8 mM/l, 100 μl), GS441524 (40 or 8 mM/l, 100 μl) and GC376 + GS441524 (20 or 4 mM/l, 100 μl) against SARS-CoV-2 in mice. In the compound-treated group, the viral RNA and viral titre were detected in the nasal turbinates and lungs on days 3 and 5 post-inoculation (p.i.); the viral RNA loads and viral titre in the nasal turbinates were not significantly decreased compared with those in the mock-treated mice on day 3 p.i (Figure 3A, B and Supplementary Figure 5A, B). Although no significant decreases in viral RNA loads were observed, high-dose GC376 + GS441524 significantly inhibited the replication of SARS-CoV-2 in the turbinate on day 5 p.i. (Figure 3C, D and Supplementary Figure 5C, D). Our results showed that high-dose GS441524 and GC376 + GS441524 completely inhibited the proliferation of SARS-CoV-2 in mouse lungs on days 3 and 5 p.i. (Figure 3E, F, G, H and Supplementary Figure 6). Besides, the virus yields in the lungs of the high-dose GC376-treated group were significantly reduced compared to mock-treated mice on day 5 p.i., but it could not completely block the viral

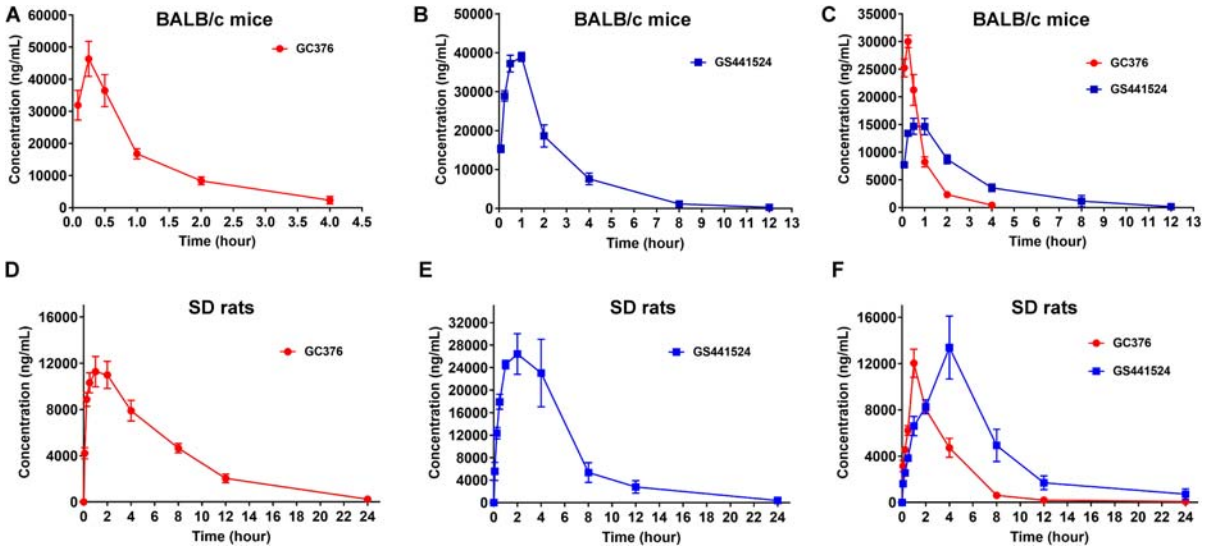

Figure 5. Plasma concentration-vs-time profiles following GC376, GS441524 and GC376 + GS441524 administration in the SPF BALB/c mice and SD rats. In the single-dose PK study, the SPF BALB/c mice and SD rats were i.m. injected with GC376 (111 mg/kg), GS441524 (67 mg/kg) and GC376 + GS441524 (55.5 + 33.5 mg/kg) for the determination of serial plasma drug concentrations. Data were analyzed via GraphPad Prism7.0, and the error bars show the SEM of the results from five replicates.

proliferation (Figure 3H and Supplementary Figure 6D). Additionally, the ability of the low-dose compound-treated group to inhibit viral replication was lower than the high-dose group in the lungs (Figure 3E, F, G, H and Supplementary Figure 6). Similar to RDV [26], high-dose GS441524 and GC376 + GS441524 completely blocked the proliferation of SARS-CoV-2 in mouse lungs, but these agents failed to block virus proliferation in the nasal turbinates on day 5 p.i. These data indicated that high-dose i.m. compound treatment (excluding GC376) efficiently inhibited the replication of SARS-CoV-2 in the lungs, but not in the nasal turbinates of BALB/c mice.

Furthermore, we assessed whether intranasal (i.n.) administration would improve the efficacy of GC376 and GS441524 to inhibit the replication of SARS-CoV-2 in the upper respiratory tract. Mice were treated with GC376 (i.n. and i.n. + i.m.), GS441524 (i.n. and i.n. + i.m.) and GC376 + GS441524 (i.n. and i.n. + i.m.). Our results showed that GS441524 and GC376 + GS441524 markedly inhibited viral replication in nasal turbinates on days 3 and 5 p.i. (Figure 4B, D and Supplementary Figure 7B, D). Only a small amount of infectious virus was detected in one mouse on day 5 p.i., although viral RNA was detected in 2 of the 3 mice in the GS441524-treated group (Figure 4C, D and Supplementary Figure 7C, D). However, i.n. administration of GS441524 did not significantly inhibit viral replication in the lungs compared to that of the mock-treated group on day 5 p.i (Figure 4G, H and Supplementary Figure 8C, D). Notably, we observed that i.n. administration of GC376 + GS441524 blocked viral replication in the lungs on day 5 p.i., although viral RNA was detected in 1 of the 3 mice (Figure 4G, H and Supplementary Figure 8C, D). GS441524 treatment via i.n. and i.m. routes completely blocked viral replication in the nasal turbinates and lungs, although viral RNAs were detected from the nasal turbinates of 2 of the 3 mice on day 3 p.i (reduced approximately 700-fold compared to that of the mock-treated group) (Figure 4 and Supplementary Figures 7 and 8). Similarly, low-dose GC376 + GS441524 treatment (i.n. + i.m.) also completely blocked viral replication in the nasal turbinates and lungs, although viral RNAs were detected from the nasal turbinates of 2 of the 3 mice on day 3 and 5 p.i. (reduced approximately 1500-fold and 263-fold compared to that of the mock-treated group, respectively) (Figure 4 and Supplementary Figures 7 and 8). Although GC376 treatment via the i.n. or combined i.n. and i.m. routes reduced the level of virus replication on day 5 p.i (Supplementary Figures 7D and 8D), it did not completely blocked viral replication in nasal turbinates and lungs (Figure 4). Furthermore, to explore the molecular mechanism of GS441524 inhibiting the SARS-CoV-2 proliferation, when GS441524 is used alone or in combination, it is necessary to use deep sequencing technology to determine the SARS-CoV-2 genome sequence in the follow-up research.

Pharmacokinetics study of GC376 and GS441524 alone or in combination

To further examine the potential of GC376 and GS441524, we evaluated their pharmacokinetic (PK) properties in SPF BALB/c mice and SD rats following i.m. administration of GC376 (111 mg/kg), GS441524 (67 mg/kg) and GC376 + GS441524 (55.5 + 33.5 mg/kg), which are the same doses according to *in vivo*

Table 1. Preliminary pharmacokinetic (PK) evaluation of GC376 and GS441524 in BALB/c mice[a].

	Compd.	Admin i.m.(mg/kg)	$t_{1/2}$ (h)	T_{max} (h)	C_{max} (μg/mL)	AUC_{0-t} (h*μg/mL)	Vd/F (mL/kg)	CL/F (mL/h/kg)	MRT_{0-t} (h)	$MRT_{0-\infty}$ (h)
alone	GC376	111	1.12 ± 0.53	0.22 ± 0.07	46.70 ± 10.69	55.29 ± 11.26	2868 ± 432	1985 ± 485	1.05 ± 0.12	1.38 ± 0.59
	GS441524	67	1.51 ± 0.16	0.80 ± 0.24	39.64 ± 2.93	106.82 ± 16.79	1367 ± 129	639 ± 119	2.07 ± 0.42	2.15 ± 0.42
combined	GC376	55.5	0.81 ± 0.22	0.25 ± 0.00	30.04 ± 0.22	27.75 ± 4.41	2339 ± 617	2031 ± 383	0.79 ± 0.09	0.88 ± 0.12
	GS441524	33.5	1.67 ± 0.24	0.55 ± 0.24	16.04 ± 2.20	48.97 ± 11.72	1678 ± 282	708 ± 136	2.37 ± 0.73	2.48 ± 0.71

[a]The value for the BALB/c mice represents the results (mean ± SD) from five independent experiments.

Table 2. Preliminary pharmacokinetic (PK) evaluation of GC376 and GS441524 in SD rats[a].

	Compd.	Admin i.m.(mg/kg)	$t_{1/2}$ (h)	T_{max} (h)	C_{max} (μg/mL)	AUC_{0-t} (h*μg/mL)	Vd/F (mL/kg)	CL/F (mL/h/kg)	MRT_{0-t} (h)	$MRT_{0-\infty}$ (h)
alone	GC376	111	3.87 ± 0.49	1.30 ± 0.60	12.56 ± 1.9	92.14 ± 9.99	6750 ± 1038	1208 ± 122	5.83 ± 0.74	6.06 ± 0.64
	GS441524	67	3.80 ± 1.17	2.00 ± 1.10	30.96 ± 8.40	183.33 ± 64.36	2251 ± 946	423 ± 186	4.50 ± 1.11	4.78 ± 1.49
combined	GC376	55.5	2.75 ± 0.91	1.40 ± 0.49	11.78 ± 1.63	42.40 ± 6.44	5165 ± 1870	1311 ± 201	2.97 ± 0.41	3.32 ± 0.57
	GS441524	33.5	5.13 ± 2.56	3.40 ± 1.20	10.52 ± 1.85	88.30 ± 26.77	2706 ± 1245	396 ± 133	6.03 ± 1.37	7.57 ± 2.93

[a]The value for the SD rats represents the results (mean ± SD) from five independent experiments.

antiviral study. In mice, the PK results showed that GC376 and GS441524 were rapidly absorbed after i.m. administration, and the peak plasma level was reached 0.22 ± 0.07 h and 0.80 ± 0.24 h after injection, respectively (Figure 5A, B and Table 1). Because the i.m. administered dose of GC376 was approximately 1.7-fold that of GS441524, we found that the maximum detected plasma drug concentration (C_{max}) of GC376 (46.70 ± 10.69 μg/ml) was approximately 1.2-fold that of GS441524 (39.64 ± 2.93 μg/ml) (Table 1). However, the value of the area under the curve (AUC_{0-t}) of GS441524 (AUC_{0-t} = 106.82 ± 16.79) was approximately 1.9-fold that of GC376 (AUC_{0-t} = 55.29 ± 11.26). Meanwhile, we observed that the clearance rate of GC376 (CL/F, 1985 ± 485 ml/h/kg) in plasma was approximately 3.1-fold that of GS441524 (CL/F, 639 ± 119 ml/h/kg) (Table 1). Besides, the PK results in SD rats showed that the T_{max} of GC376 and GS441524 were 1.30 ± 0.60 h and 2.00 ± 1.10 h, respectively (Figure 5D, E and Table 2). Compared with mice, the utilization efficiency of GS441524 *in vivo* is significantly higher than that of GC376 in SD rats. We found that the maximum detected plasma drug concentration (C_{max}) of GC376 (12.56 ± 1.90 μg/ml) was approximately 2.5-fold lower than GS441524 (30.96 ± 8.40 μg/ml) (Table 2). The value of the area under the curve (AUC_{0-t}) of GS441524 (AUC_{0-t} = 183.33 ± 64.36) was approximately 2.0-fold higher than GC376 (AUC_{0-t} = 92.14 ± 9.99). We also observed that the clearance rate of GC376 (CL/F, 1208 ± 122 ml/h/kg) in plasma was approximately 2.9-fold that of GS441524 (CL/F, 423 ± 186 ml/h/kg) (Table 2).

These results indicated that the utilization efficiency of GS441524 *in vivo* is significantly higher than that of GC376. This finding may be one of the reasons for the poor ability of GC376 to inhibit SARS-CV-2 *in vivo*. The previous results showed that GC376 targeting the FIPV 3CLpro could effectively reduce the virus load in the macrophages from the ascites of cats with the duration of antiviral treatment [17,19]. Therefore, we speculate that GC376 can effectively inhibit the proliferation of coronaviruses (FIPV and SARS-CoV-2), but cannot quickly clear the virus from infected tissues. During continuous administration, GC376 needs to maintain an effective concentration for a long time to inhibit virus proliferation in the infected tissue. However, compared with GS441524, GC376 could be quickly cleared in the BALB/c mice and SD rats. Besides, the nasal turbinate and lung are the main target organs for SARS-CoV-2 proliferation, there is a large amount of SARS-CoV-2 in these tissues. Therefore, it is difficult for GC376 to completely inhibit the proliferation of SARS-CoV-2 in the mice nasal turbinates and lungs.

Furthermore, we found that the combined application of GC376 and GS441524 extended $T_{1/2}$ from 1.51 ± 0.16 h to 1.67 ± 0.24 h and the residence time of GS441524 (MRT_{0-t} from 2.07 ± 0.42 h to 2.37 ± 0.73 h) in SPF BALB/c mice (Figure 5C and Table 1). Similarly, the PK results showed that the combined application of GC376 and GS441524 extended $T_{1/2}$ from 3.80 ± 1.17 h to 5.13 ± 2.56 h and the residence time of GS441524 (MRT_{0-t} from 4.50 ± 1.11 h to 6.03 ± 1.37 h) in SPF SD rats (Figure 5F and Table 2). Moreover, the PK study results showed that GC376 reached C_{max} earlier (T_{max} = 0.25 h in mice and T_{max} = 1.40 ± 0.49 h in SD rats) than GS441524 (T_{max} = 0.55 ± 0.24 h in mice and T_{max} = 3.40 ± 1.20 h in SD rats) to produce a synergistic effect (Figure 5C, F). When these agents were combined, GC376 was the first drug to inhibit SARS-CoV-2 replication. After the plasma concentration of GC376 decreased, GS441524 reached its C_{max} (Figure 5C, F and Tables 1 and 2) to produce a continuous inhibition of SARS-CoV-2 proliferation and maintain the effective concentration for a longer time. This phenomenon may explain why the combined application of GC376 and GS441524 was better than single application alone.

In summary, we assessed the efficacy of GC376 and GS441524 to inhibit SARS-CoV-2 replication using a mouse-adapted virus infection model. Importantly, we found that intranasal administration of GS441524 and GC376 + GS441524 significantly prevents the replication of virus in the upper respiratory tract, and the efficacy of GC376 + GS441524 to inhibit the viral replication in the lower respiratory tract significantly better than that of GS441524. Combined i.n. and i.m. administration of GS441524 and GC376 + GS441524 effectively protected mice against HRB26M infection in the upper and lower respiratory tracts, but GC376 alone failed to block the proliferation of SARS-CoV-2 in mice. Compared with GC376 and GS441524 alone, the dosage of GC376 + GS441524 is halved, these results showed an additive effect of the combined application of the M^{pro} and RdRp inhibitors, so it should be developed and considered for future clinic practice.

Acknowledgments

We thank research associates at the Center for Protein Research (CPR), Huazhong Agricultural University, for technical support. We also thank Professor Sheng-ce Tao from Shanghai Jiao Tong University for providing SARS-CoV-2 M^{pro} plasmid. This work was supported by National Natural Science Foundation of China Grants 31722056 and 31802207, the National Key R&D Program of China (grant number 2018YFC1200601), the Natural Science Foundation of Hubei Province of China (grant number2020FCA040), the Fundamental Research Funds for the Central Universities (grant number2662020PY001) and the Applied Technology Research and Development Project of Heilongjiang Province, China (grant number GA20C006).

Disclosure statement

No potential conflict of interest was reported by the author (s).

Funding

This work was supported by National Natural Science Foundation of China Grants 31873020, 31802207 and 31722056, the National Key R&D Program of China (grant number 2018YFC1200601), the Natural Science Foundation of Hubei Province of China (grant number 2020FCA040), the Fundamental Research Funds for the Central Universities (grant number 2662020PY001) and the Applied Technology Research and Development Project of Heilongjiang Province, China (grant number GA20C006).

ORCID

Yuejun Shi http://orcid.org/0000-0002-9500-6995
Lei Shuai http://orcid.org/0000-0003-2122-8365
Zhiyuan Wen http://orcid.org/0000-0003-3112-0243
Chong Wang http://orcid.org/0000-0002-3970-9071
Yuanyuan Yan http://orcid.org/0000-0001-8385-8827
Zhe Jiao http://orcid.org/0000-0002-0250-0565
Fenglin Guo http://orcid.org/0000-0001-8122-0176
Zhen F. Fu http://orcid.org/0000-0001-6293-9329
Huanchun Chen http://orcid.org/0000-0003-0680-5953
Zhigao Bu http://orcid.org/0000-0001-9242-4211
Guiqing Peng http://orcid.org/0000-0001-8813-6663

References

[1] Gao Q, Bao L, Mao H, et al. Development of an inactivated vaccine candidate for SARS-CoV-2. Science. 2020 Jul;369(6499):77–81.
[2] van Doremalen N, Lambe T, Spencer A, et al. ChAdOx1 nCoV-19 vaccine prevents SARS-CoV-2 pneumonia in rhesus macaques. Nature. 2020 Oct;586(7830):578–582.
[3] Yu J, Tostanoski LH, Peter L, et al. DNA vaccine protection against SARS-CoV-2 in rhesus macaques. Science. 2020 Aug;369(6505):806–811.
[4] Wu S, Zhong G, Zhang J, et al. A single dose of an adenovirus-vectored vaccine provides protection against SARS-CoV-2 challenge. Nat Commun. 2020 Aug;11 (1):4081.
[5] Zhu FC, Li YH, Guan XH, et al. Safety, tolerability, and immunogenicity of a recombinant adenovirus type-5 vectored COVID-19 vaccine: a dose-escalation, open-label, non-randomised, first-in-human trial. Lancet. 2020 Jun;395(10240):1845–1854.
[6] Zhu FC, Guan XH, Li YH, et al. Immunogenicity and safety of a recombinant adenovirus type-5-vectored COVID-19 vaccine in healthy adults aged 18 years or older: a randomised, double-blind, placebo-controlled, phase 2 trial. Lancet. 2020 Aug;396 (10249):479–488.
[7] Gorbalenya AE, Enjuanes L, Ziebuhr J, et al. Nidovirales: evolving the largest RNA virus genome. Virus Res. 2006 Apr;117(1):17–37.
[8] Perlman S, Netland J. Coronaviruses post-SARS: update on replication and pathogenesis. Nat Rev Microbiol. 2009 Jun;7(6):439–450.
[9] de Wilde AH, Snijder EJ, Kikkert M, et al. Host factors in coronavirus replication. Curr Top Microbiol Immunol. 2018;419:1–42.
[10] Yin W, Mao C, Luan X, et al. Structural basis for inhibition of the RNA-dependent RNA polymerase from SARS-CoV-2 by remdesivir. Science. 2020 Jun;368 (6498):1499–1504.
[11] Ye G, Wang X, Tong X, et al. Structural basis for inhibiting porcine epidemic diarrhea virus replication with the 3C-Like protease inhibitor GC376. Viruses. 2020 Feb;12(2):240.
[12] Ma C, Sacco MD, Hurst B, et al. Boceprevir, GC-376, and calpain inhibitors II, XII inhibit SARS-CoV-2 viral replication by targeting the viral main protease. Cell Res. 2020 Aug;30(8):678–692.
[13] Fu L, Ye F, Feng Y, et al. Both Boceprevir and GC376 efficaciously inhibit SARS-CoV-2 by targeting its main protease. Nat Commun. 2020 Sep;11(1):4417.
[14] Kim Y, Lovell S, Tiew KC, et al. Broad-spectrum antivirals against 3C or 3C-like proteases of picornaviruses, noroviruses, and coronaviruses. J Virol. 2012 Nov;86(21):11754–11762.
[15] Tiew KC, He G, Aravapalli S, et al. Design, synthesis, and evaluation of inhibitors of norwalk virus 3C protease. Bioorg Med Chem Lett. 2011 Sep;21(18):5315–5319.
[16] Vuong W, Khan MB, Fischer C, et al. Feline coronavirus drug inhibits the main protease of SARS-CoV-2 and blocks virus replication. Nat Commun. 2020 Aug;11(1):4282.
[17] Kim Y, Mandadapu SR, Groutas WC, et al. Potent inhibition of feline coronaviruses with peptidyl compounds targeting coronavirus 3C-like protease. Antiviral Res. 2013 Feb;97(2):161–168.
[18] Mandadapu SR, Weerawarna PM, Gunnam MR, et al. Potent inhibition of norovirus 3CL protease by peptidyl α-ketoamides and α-ketoheterocycles. Bioorg Med Chem Lett. 2012 Jul;22(14):4820–4826.
[19] Kim Y, Liu H, Galasiti Kankanamalage AC, et al. Reversal of the progression of fatal coronavirus infection in cats by a broad-spectrum coronavirus protease inhibitor. PLoS Pathog. 2016 Mar;12(3):e1005531.
[20] Agostini ML, Andres EL, Sims AC, et al. Coronavirus susceptibility to the antiviral remdesivir (GS-5734) is mediated by the viral polymerase and the proofreading exoribonuclease. mBio. 2018 Mar;9(2):e00221-18.
[21] Cho A, Saunders OL, Butler T, et al. Synthesis and antiviral activity of a series of 1'-substituted 4-aza-7,9-dideazaadenosine C-nucleosides. Bioorg Med Chem Lett. 2012 Apr;22(8):2705–2707.
[22] Sheahan TP, Sims AC, Graham RL, et al. Broad-spectrum antiviral GS-5734 inhibits both epidemic and zoonotic coronaviruses. Sci Transl Med. 2017 Jun;9 (396):eaal3653.
[23] Warren TK, Jordan R, Lo MK, et al. Therapeutic efficacy of the small molecule GS-5734 against Ebola virus in rhesus monkeys. Nature. 2016 Mar;531 (7594):381–385.
[24] Yan VC, Muller FL. Advantages of the parent nucleoside GS-441524 over remdesivir for covid-19 treatment. ACS Med Chem Lett. 2020 Jul;11(7):1361–1366.
[25] Wang M, Cao R, Zhang L, et al. Remdesivir and chloroquine effectively inhibit the recently emerged novel coronavirus (2019-nCoV) in vitro. Cell Res. 2020 Mar;30(3):269–271.
[26] Wang J, Shuai L, Wang C, et al. Mouse-adapted SARS-CoV-2 replicates efficiently in the upper and lower

respiratory tract of BALB/c and C57BL/6J mice. Protein Cell. 2020 Oct;11(10):776–782.
[27] Tempestilli M, Caputi P, Avataneo V, et al. Pharmacokinetics of remdesivir and GS-441524 in two critically ill patients who recovered from COVID-19. J Antimicrob Chemother. 2020 Oct;75 (10):2977–2980.
[28] Sheahan TP, Sims AC, Leist SR, et al. Comparative therapeutic efficacy of remdesivir and combination lopinavir, ritonavir, and interferon beta against MERS-CoV. Nat Commun. 2020 Jan;11(1):222.
[29] de Wit E, Feldmann F, Cronin J, et al. Prophylactic and therapeutic remdesivir (GS-5734) treatment in the rhesus macaque model of MERS-CoV infection. Proc Natl Acad Sci U S A. 2020 Mar;117(12):6771–6776.
[30] Choy KT, Wong AY, Kaewpreedee P, et al. Remdesivir, lopinavir, emetine, and homoharringtonine inhibit SARS-CoV-2 replication in vitro. Antiviral Res. 2020 Jun;178:104786.
[31] Murphy BG, Perron M, Murakami E, et al. The nucleoside analog GS-441524 strongly inhibits feline infectious peritonitis (FIP) virus in tissue culture and experimental cat infection studies. Vet Microbiol. 2018 Jun;219:226–233.
[32] Shi Y, Li Y, Lei Y, et al. A dimerization-dependent mechanism drives the endoribonuclease function of Porcine Reproductive and Respiratory syndrome virus nsp11. J Virol. 2016 May;90(9):4579–4592.
[33] Shi Y, Tong X, Ye G, et al. Structural characterization of the helicase nsp10 encoded by porcine reproductive and respiratory syndrome virus. J Virol. 2020 Jul;94 (15):e02158-19.
[34] Minor W, Cymborowski M, Otwinowski Z, et al. HKL-3000: the integration of data reduction and structure solution–from diffraction images to an initial model in minutes. Acta Crystallogr D Biol Crystallogr. 2006 Aug;62(Pt 8):859–866.
[35] Adams PD, Grosse-Kunstleve RW, Hung LW, et al. PHENIX: building new software for automated crystallographic structure determination. Acta Crystallogr D Biol Crystallogr. 2002 Nov;58(Pt 11):1948–1954.
[36] Emsley P, Cowtan K. Coot: model-building tools for molecular graphics. Acta Crystallogr D Biol Crystallogr. 2004 Dec;60(Pt 12 Pt 1):2126–2132.
[37] Laskowski RA, Swindells MB. Ligplot+: multiple ligand-protein interaction diagrams for drug discovery. J Chem Inf Model. 2011 Oct;51(10):2778–2786.
[38] Pedersen NC, Kim Y, Liu H, et al. Efficacy of a 3C-like protease inhibitor in treating various forms of acquired feline infectious peritonitis. J Feline Med Surg. 2018 Apr;20(4):378–392.
[39] Kim Y, Shivanna V, Narayanan S, et al. Broad-spectrum inhibitors against 3C-like proteases of feline coronaviruses and feline caliciviruses. J Virol. 2015 May;89(9):4942–4950.
[40] Perera KD, Galasiti Kankanamalage AC, Rathnayake AD, et al. Protease inhibitors broadly effective against feline, ferret and mink coronaviruses. Antiviral Res. 2018 Dec;160:79–86.
[41] Pruijssers AJ, George AS, Schäfer A, et al. Remdesivir inhibits SARS-CoV-2 in human lung cells and chimeric SARS-CoV expressing the SARS-CoV-2 RNA polymerase in mice. Cell Rep. 2020 Jul;32 (3):107940.
[42] Tchesnokov EP, Feng JY, Porter DP, et al. Mechanism of inhibition of Ebola virus RNA-dependent RNA polymerase by remdesivir. Viruses. 2019 Apr;11 (4):326.
[43] Gordon CJ, Tchesnokov EP, Woolner E, et al. Remdesivir is a direct-acting antiviral that inhibits RNA-dependent RNA polymerase from severe acute respiratory syndrome coronavirus 2 with high potency. J Biol Chem. 2020 May;295 (20):6785–6797.
[44] Wang Q, Wu J, Wang H, et al. Structural Basis for RNA replication by the SARS-CoV-2 polymerase. Cell. 2020 Jul;182(2):417–428.e13.
[45] Kokic G, Hillen HS, Tegunov D, et al. Mechanism of SARS-CoV-2 polymerase stalling by remdesivir. Nat Commun. 2021 Jan;12(1):279.